Supplemental Data

Stable Benzotriazole Esters

as Mechanism-Based Inactivators of the

Severe Acute Respiratory Syndrome 3CL Protease

Chung-Yi Wu, Ke-Yung King, Chih-Jung Kuo, Jim-Min Fang, Ying-Ta Wu, Ming-Yi Ho, Chung-Lin Liao, Jiun-Jie Shie, Po-Huang Liang, and Chi-Huey Wong

90 Acids

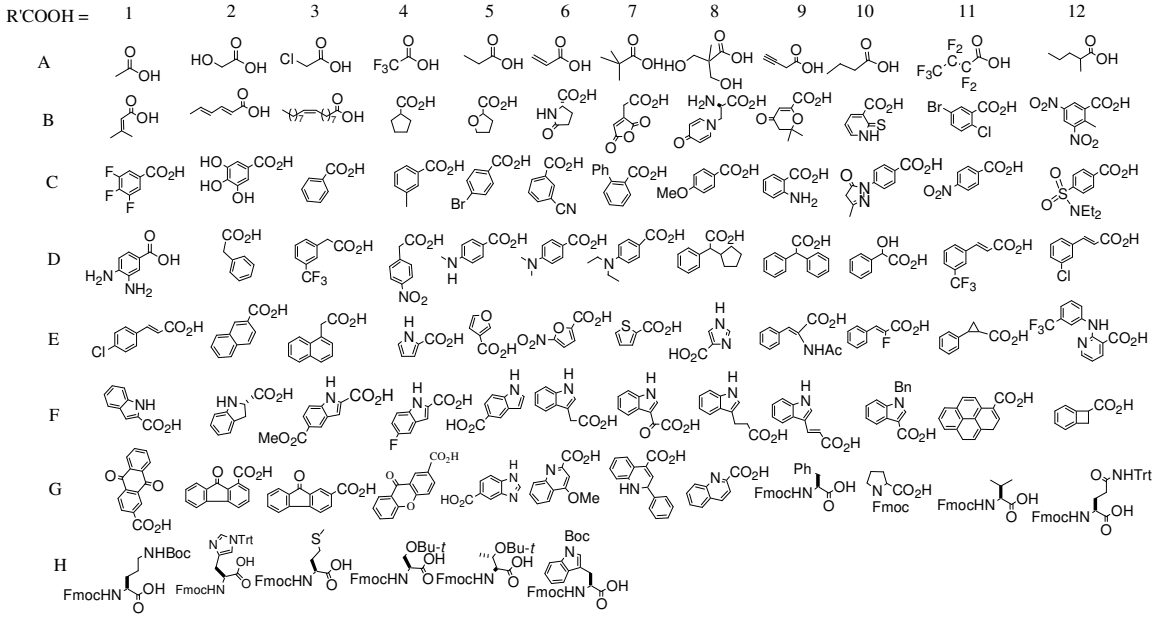

Synthesis and characterization of compounds 15-20

1-(4-Amimo-phenyl)-2-benzotriazol-yl-ethanone (15) and 1-(4-Amimo-phenyl)-2-benzotriazol-yl-ethanol (16). Compound **13** (0.50 g, 1.77 mmol) was dissolved in MeOH (15 mL) and palladium hydroxide (10 mg) was added. The reaction mixture was stirred at rt under 1 atm of H_2 for 3 h. After the palladium hydroxide was filtered and the solvent removed im a vacuum, the product was purified by silica gel column to get 0.37 g compound **15** (82 %) and 58.5 mg compound **16** (13%) as white solids. **(15)** ^{1}H NMR ($CDCl_3$, 400 MHz) δ = 7.18 (d, *J* = 4.8 Hz, 1H), 7.06 (d, *J* = 6.8 Hz, 2H), 6.84 (d, *J* = 6.8 Hz, 1H), 6.64 (dd, *J* = 5.6 Hz, *J* = 5.6 Hz, 1H), 6.53 (dd, *J* = 5.6 Hz, *J* = 5.6 Hz, 1H), 5.92 (d, *J* = 6.8 Hz, 2H), 5.40 (s, 2H), 4.90 (s, 2H). ^{13}C NMR (d_6-acetone, 100 MHz) δ 190.09, 156.21, 147.73, 136.23, 132.56, 128.83, 125.29, 124.89, 121.06, 114.94, 112.41, 54.90; ESI-MS [M + 1]calculated for $C_{14}H_{12}N_4O$ 253.10, found 253.17. **(16)** ^{1}H NMR ($CDCl_3$, 400 MHz) δ = 7.86 (d, *J* = 6.8 Hz, 1H), 7.51 (d, *J* = 6.4 Hz, 1H), 7.40 (dd, *J* = 5.6 Hz, *J* = 5.6 Hz, 1H), 7.27 (dd, *J* = 5.6 Hz, *J* = 5.6 Hz, 1H), 6.59 (d, *J* = 6.8 Hz, 2H), 5.16 (t, *J* = 3.6 Hz, 1H), 4.72 (s, 2H), 4.68 (d, *J* = 3.6Hz, 2H), 3.71(s,1H).^{13}C NMR (d_6-acetone,100MHz) δ 146.40, 145.31, 133.66, 130.36, 127.14, 126.94, 123.79, 119.32, 115.16, 110.08, 73.00, 55.45; ESI-MS [M + 1] calculated for $C_{14}H_{14}N_4O$ 255.12, found 255.11.

General procedure for the TBAF assisted monomethylation or dimethylation: 2-Benzotrizaole-1-yl-1-(4-methylamino-phenyl)-ethanone (17) and 2-Benzotrizaole-1-yl-1-(4-dimethylamino-phenyl)-ethanone (18). Compound **15** (0.40 g, 1.59 mmol) and methyl iodide (0.27 g, 1.90 mmol, 1.2 equiv) were placed in a 10 mL flask with a stirring bar followed by the addition of TBAF (1.9 mL, 1.9 mmol, 1.2 equiv, 1M in THF) at room temperature. After being stirred for 6 h at room temperature, the reaction was directly loaded into the column and the product was eluted with solution of 3:1 hexane: ethyl acetate to yield 0.26 g of product **17** (65%) and 0.10 g of product **18** (23%) as a pale yellow solid. Compound **17**: ^{1}H NMR ($CDCl_3$, 400 MHz) δ = 8.02 (d, *J* = 5.6 Hz, 1H), 7.88 (d, *J* = 8.4 Hz, 2H), 7.56 (d, J = 6.8 Hz, 1H), 7.41 (dd, *J* = 5.6 Hz, *J* = 6.8 Hz, 1H), 7.32 (dd, *J* = 6.8 Hz, *J* = 6.8 Hz, 1H), 6.64 (q, J = 6.0 Hz, 1H), 6.57 (d, *J* = 8.4 Hz, 2H), 4.19 (s, 2H), 1.94 (d, J = 6.0 Hz, 3H). ^{13}C NMR (d_6-acetone,100MHz) δ 189.76, 155.76, 148.73, 139.27, 133.10, 128.98, 126.03, 12501, 121.3, 115.07, 112.61, 55.30, 29.78; ESI-MS [M + 1] calculated for $C_{15}H_{14}N_4O$ 267.12, found 267.08. Compound **18**: ^{1}H NMR ($CDCl_3$, 400 MHz) δ = 8.06 (d, *J* = 6.4 Hz, 1H), 7.94 (d, *J* = 7.2 Hz, 2H), 7.45 (d, *J* = 5.6 Hz, 1H), 7.37 (dd, *J* = 5.6 Hz, *J* = 5.6 Hz, 1H), 7.34 (dd, *J* = 5.6 Hz, J = 6.4 Hz, 1H), 6.66 (d, *J* = 7.2 Hz, 2H), 6.00 (s, 2H), 3.07 (s, 6H).^{13}C NMR ($CDCl_3$, 100 MHz) δ = 187.81, 154.10, 145.96, 133.91, 130.60, 127.60, 123.91, 121.63, 119.85, 110.87, 109.95. 53.40, 39.96; ESI-MS [M + 1]calculated for $C_{16}H_{16}N_4O$ 281.13, found 281.17.

2-Benzotrizaole-1-yl-1-(4-methylamino-phenyl)-ethanol (19) and 2-Benzotrizaole-1-yl-1-(4-dimethylamino-phenyl)-ethanol (20). The standard procedure was used. Compound **16** (0.30 g, 1.2 mmol) and methyl iodide (0.2 g, 1.44mmol, 1.2 equiv) were placed in a 10 mL flask with a stirring bar followed by the addition of TBAF (1.44mL, 1.44 mmol, 1.2 equiv, 1M in THF) at room temperature. After being stirred for 6 h at room temperature, the reaction was directly loaded into the column and the product was

eluted with solution of 3:1 hexane: ethyl acetate to yield 0.2 g of product **19** (62%) and 67.7 mg of product **20** (20%) as a pale yellow solid. Compound **19** ^{1}H NMR (d_4-Methanol, 400 MHz) δ = 7.94 (d, *J* =6.8 Hz, 1H), 7.58 (d, *J* = 6.8 Hz, 1H), 7.46 (dd, *J* = 5.6 Hz, *J* = 6.8 Hz, 1H), 7.37 (dd, *J* = 5.7 Hz, *J* = 6.8 Hz, 1H), 7.15 (d, *J* = 6.8 Hz, 2H), 6.59 (d, *J* = 6.8 Hz, 2H), 5.11 (dd, *J* = 8.4 Hz, *J* = 4.0 Hz, 1H), 4.85 (ABq, *J* = 11.6 Hz, *J* = 6.4 Hz, 1H), 4.78 (ABq, *J* = 11.6 Hz, *J* = 6.4 Hz, 1H), 2.77 (s, 3H). ^{13}C NMR (d_4-Methanol, 100 MHz) δ149.23, 144.47, 134.76, 131.25, 128.94, 127.24, 125.81, 119.72, 116.06, 109.65, 72.87, 54.76, 29.51; ESI-MS [M + 1] calculated for $C_{15}H_{16}N_4O$ 269.13, found 269.08. **(20)** ^{1}H NMR (d_4-Methanol, 400 MHz) δ = 8.03 (d, *J* = 6.8 Hz, 1H), 7.87 (d, *J* = 6.4 Hz, 1H), 7.56 (dd, *J* = 5.6 Hz, *J* = 5.6 Hz, 1H), 7.30 (dd, *J* = 5.6 Hz, *J* = 5.6 Hz, 1H), 6.61 (d, *J* = 6.8 Hz, 2H), 5.34 (t, *J* = 3.6 Hz, 1H), 4.68 (d, *J* = 3.6Hz, 2H), 3.85(s,1H), 2.97 (s, 6H).^{13}CNMR (d_4-Methanol,100MHz) δ 148.63, 146.73, 134.34, 139.28, 127.76, 127.31, 122.05, 119.65, 115.78, 110.45, 72.76, 56.76, 29.32; ESI-MS [M + 1] calculated for $C_{16}H_{18}N_4O$ 282.15, found 282.14.

Characterization of Slow Inhibitor

The protocol of kinetic measurements of a time-dependent inhibitor was followed [S1]. The progress curves of the SARS-CoV protease reactions in the presence of varying concentrations of the time-dependent inhibitor were measured using the fluorogenic substrate [S2-S4]. The reaction was initiated by adding 0.05 μM enzyme to a mixture containing 6 μM substrate and 0.3 to 3 μM inhibitor. Over the entire 5-min time window, the uninhibited enzyme displayed a linear progress curve, whereas the inhibited enzyme with different concentration of inhibitor showed a time-dependent reduction of reaction velocity (Figure 1). A higher inhibitor concentration, the reaction velocity was lower. This indicates the inhibitor is either slow-binding or slow-inactivating inhibitor.

Involvement of Cys in Slow Inhibition

The enzyme was preincubated with different concentrations (0.03-0.3 μM) of inhibitor and then a small aliquot (100 μL) of the solution was taken periodically for initial velocity assay (final enzyme concentration =0.05 μM) using the 6 μM fluorogenic substrate. The total volume we used to do the activity assay was 1.2 mL. For initial velocity measurements, the increase of the substrate fluorescence at 538 nm was monitored for the first 300 s of the reaction. The reduction of enzyme activity with the incubation time with the inhibitor was fitted with a single exponential equation to obtain the k_{obs} of inactivation at different inhibitor concentration. The small k_{obs} value suggests that the inhibitor is a slow inhibitor.

Measurements of K_i and k_{inact}

In the K_i measurement, 20-200 nM of inhibitor was used to inhibit 15 nM enzyme for all of the measurements. The inhibitor was not used in large excess since the enzyme concentration below 15 nM was hardly detected.

From the k_{obs} of inactivation, the half-life ($t_{1/2}$) can be calculated (ln 2/ k_{obs} = $t_{1/2}$). The half-life for inactivation at each inactivator concentration is plotted against 1/[inactivator] (known as Kitz and Wilson plot [S5]). A linear line can be obtained from the plot of our data (Figure 1-7). The point of intersection at the y-axis is ln $2/k_{inact}$, from which the value of k_{inact} can be determined. The extrapolated negative x axis intercept is $-1/K_i$.

Figure S1. Inhibition of $3CL^{pro}$ by Compound **3**

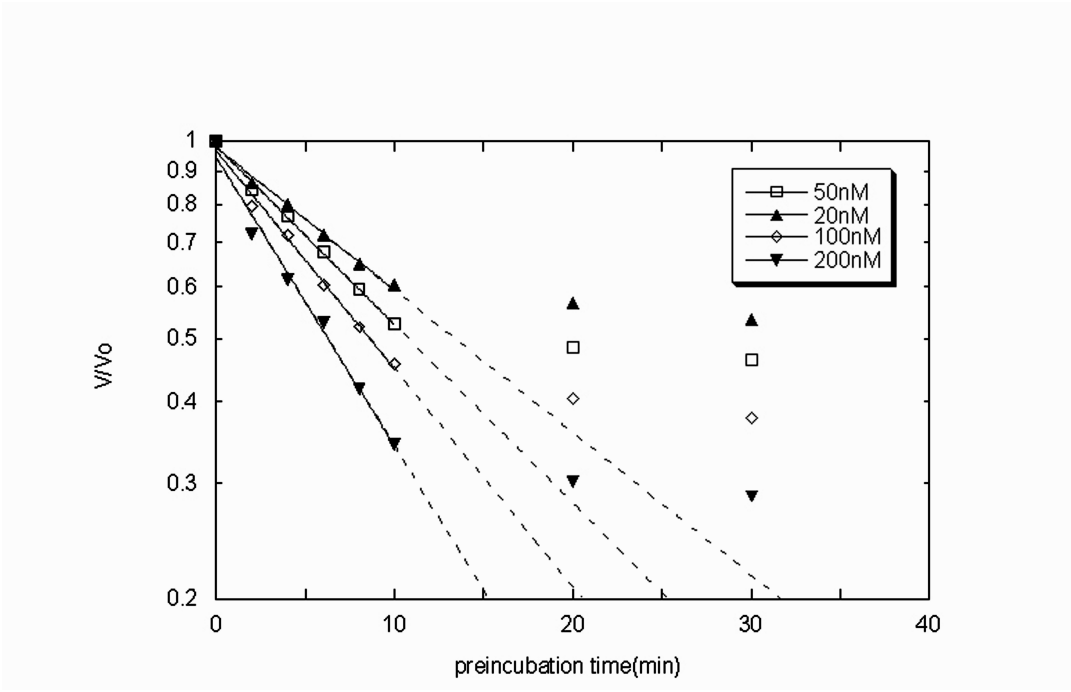

y = 0.97608 * e^(-0.050058x) R= 0.9948

y = 0.9816 * e^(-0.06275x) R= 0.99676

y = 0.96627 * e^(-0.076644x) R= 0.99396

y = 0.94471 * e^(-0.10143x) R= 0.98958

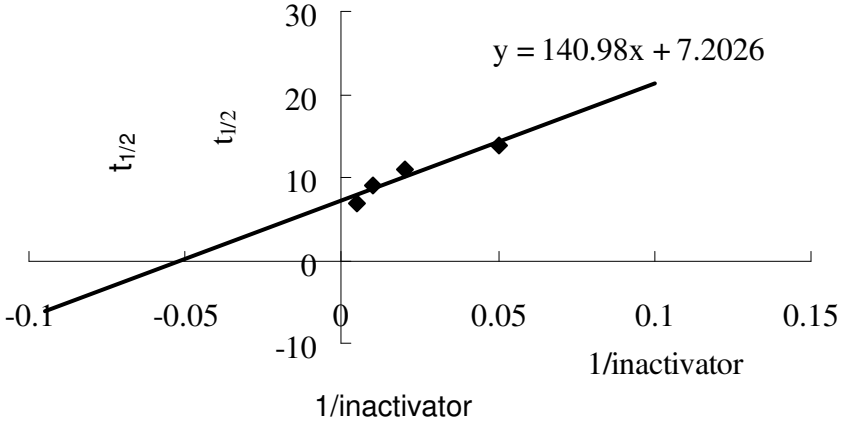

$k_{inact} = 0.0016\ s^{-1}$

$K_i = 19.5$ nM

Figure S2. Inhibition of $3CL^{pro}$ by Compound **5**

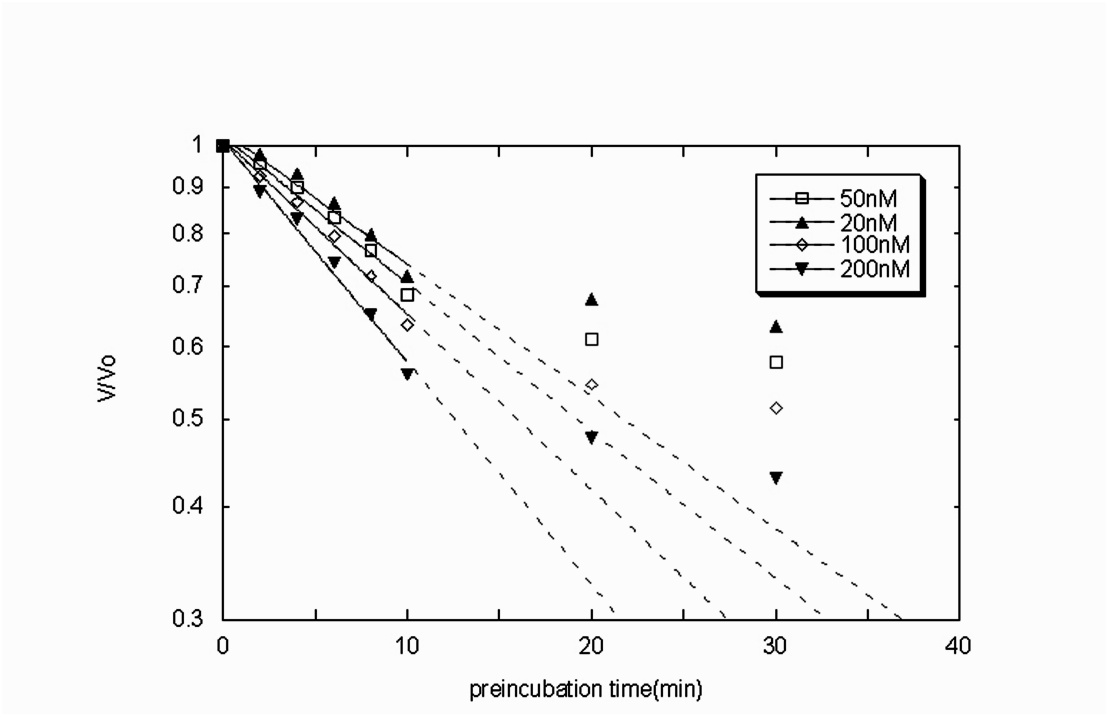

y = 1.0355 * e^(-0.033579x) R= 0.97602

y = 1.0247 * e^(-0.03742x) R= 0.98907

y = 1.0166 * e^(-0.044517x) R= 0.99406

y = 1.0142 * e^(-0.056417x) R= 0.99392

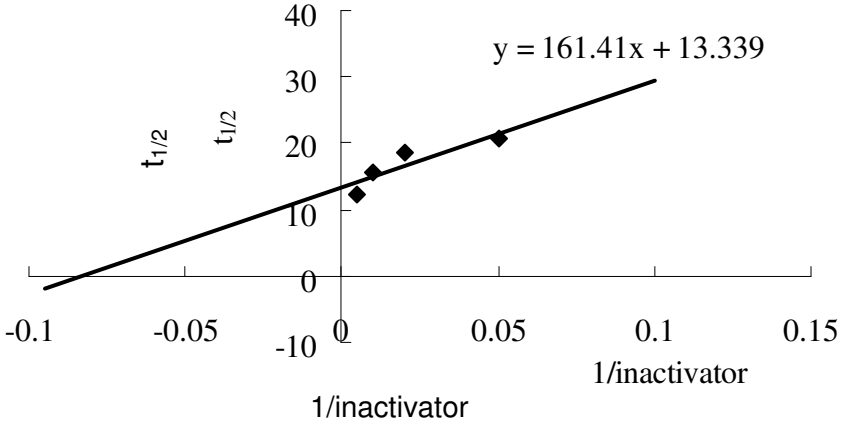

$k_{inact} = 0.0009\ s^{-1}$

$K_i = 12.1$ nM

Figure S3. Inhibition of $3CL^{pro}$ by Compound **6**

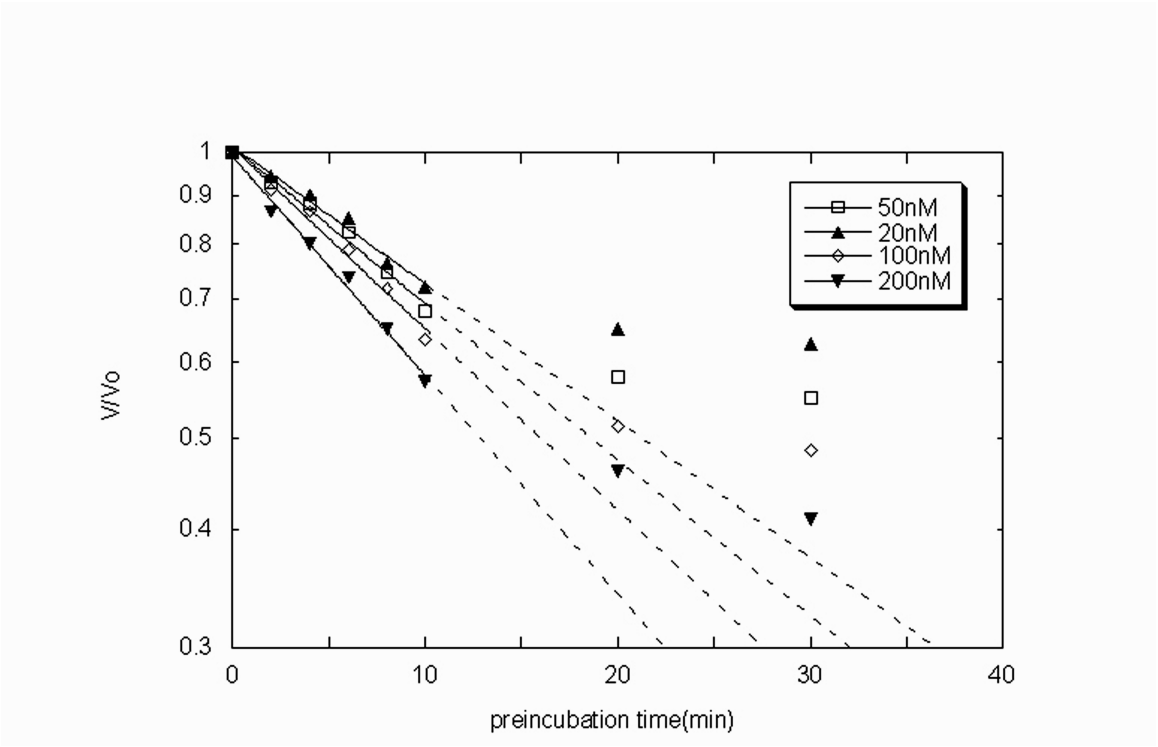

y = 1.0137 * e^(-0.033346x) R= 0.99039

y = 1.0113 * e^(-0.037927x) R= 0.99434

y = 1.011 * e^(-0.044047x) R= 0.99388

y = 0.98976 * e^(-0.053225x) R= 0.99528

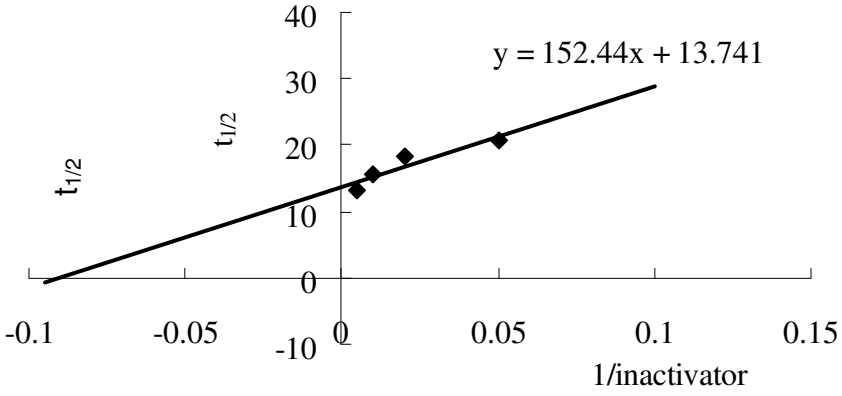

$k_{inact} = 0.0008\ s^{-1}$

$K_i = 11.1$ nM

Figure S4. Inhibition of $3CL^{pro}$ by Compound **7**

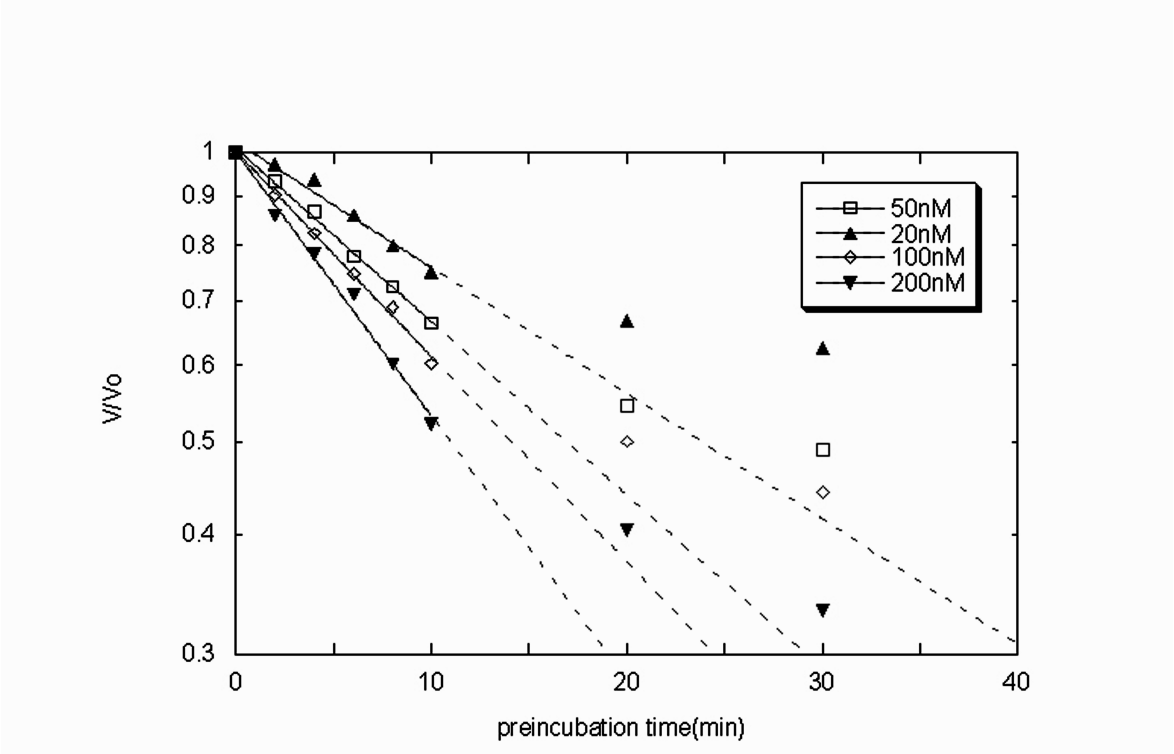

y = 1.0246 * e^(-0.030143x) R= 0.9849
y = 1.0093 * e^(-0.041569x) R= 0.99816
y = 1.0017 * e^(-0.049211x) R= 0.99844
y = 1.0002 * e^(-0.063236x) R= 0.99574

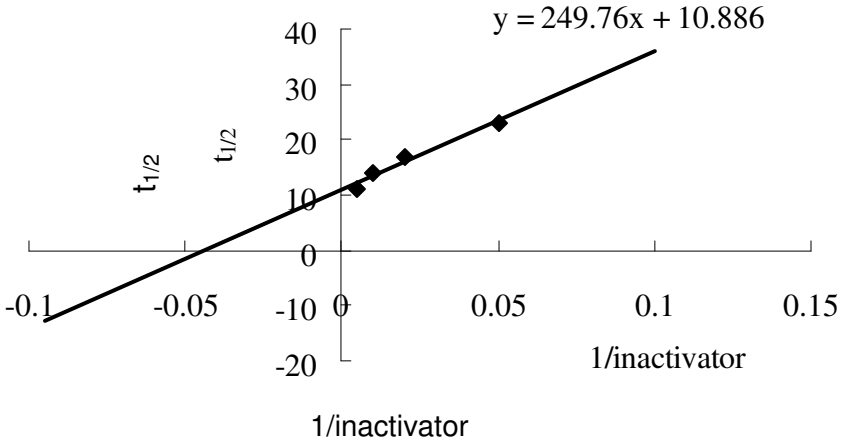

1/inactivator

$k_{inact} = 0.0011\ s^{-1}$
$K_i = 22.9$ nM

Figure S5. Inhibition of $3CL^{pro}$ by Compound **8**

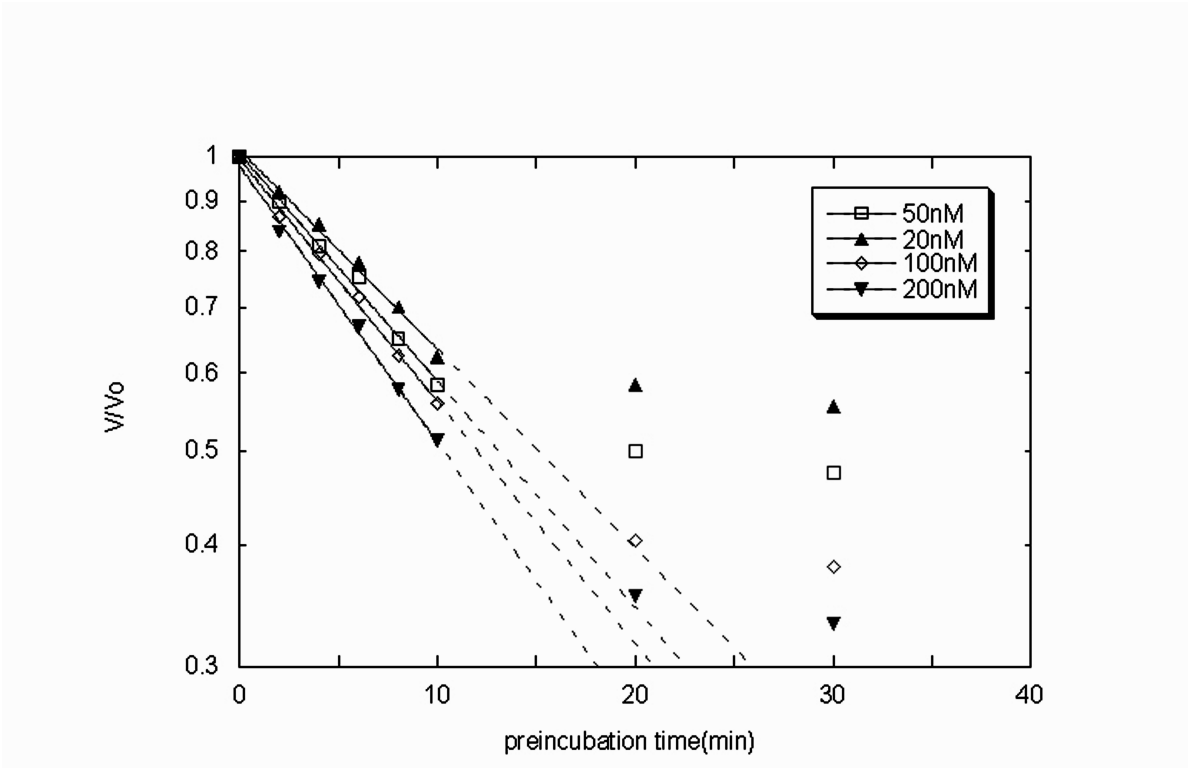

y = 1.0143 * e^(-0.046928x) R= 0.99662

y = 1.0061 * e^(-0.053566x) R= 0.99747

y = 0.99342 * e^(-0.057202x) R= 0.99777

y = 0.97838 * e^(-0.065326x) R= 0.99673

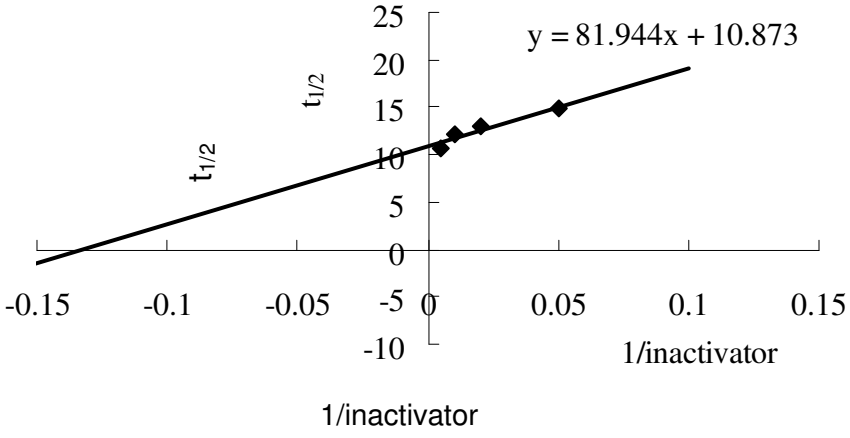

1/inactivator

$k_{inact} = 0.0011\ s^{-1}$

$K_i = 7.5$ nM

Figure S6. Inhibition of $3CL^{pro}$ by Compound **9**

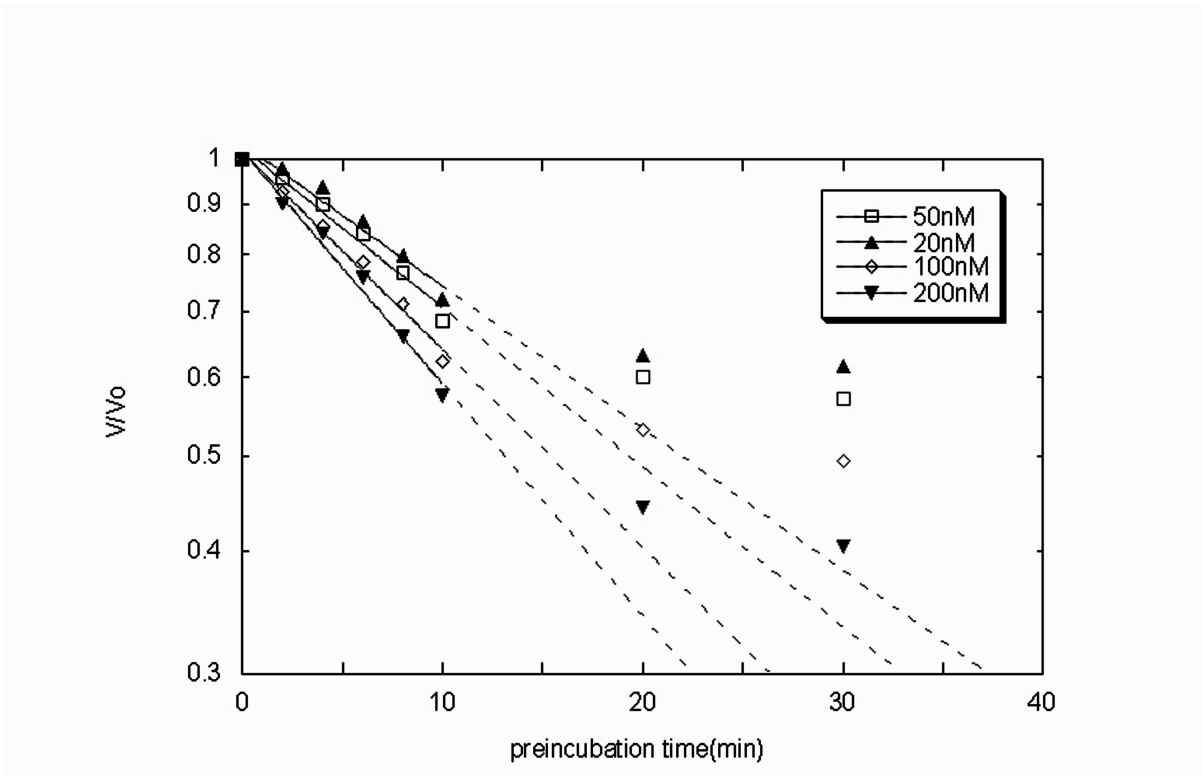

y = 1.0351 * e^(-0.033227x) R= 0.9761
y = 1.0255 * e^(-0.037301x) R= 0.98739
y = 1.0164 * e^(-0.046237x) R= 0.99507
y = 1.0185 * e^(-0.054399x) R= 0.99324

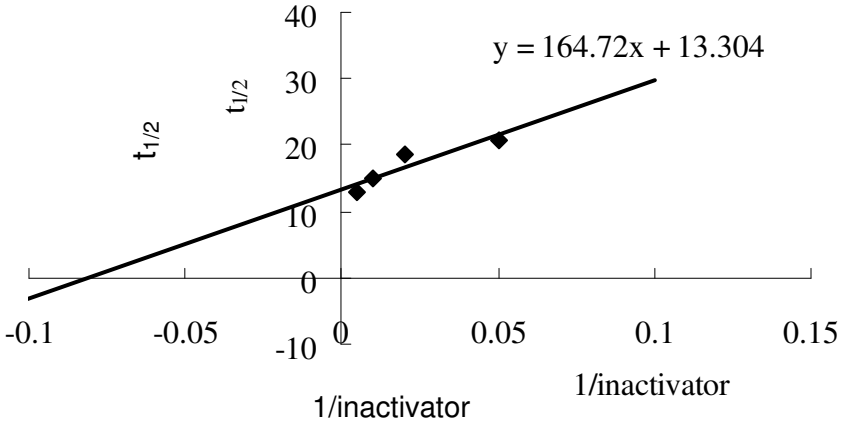

$k_{inact} = 0.0009\ s^{-1}$
$K_i = 12.3$ nM

Figure S7. Inhibition of $3CL^{pro}$ by Compound **10**

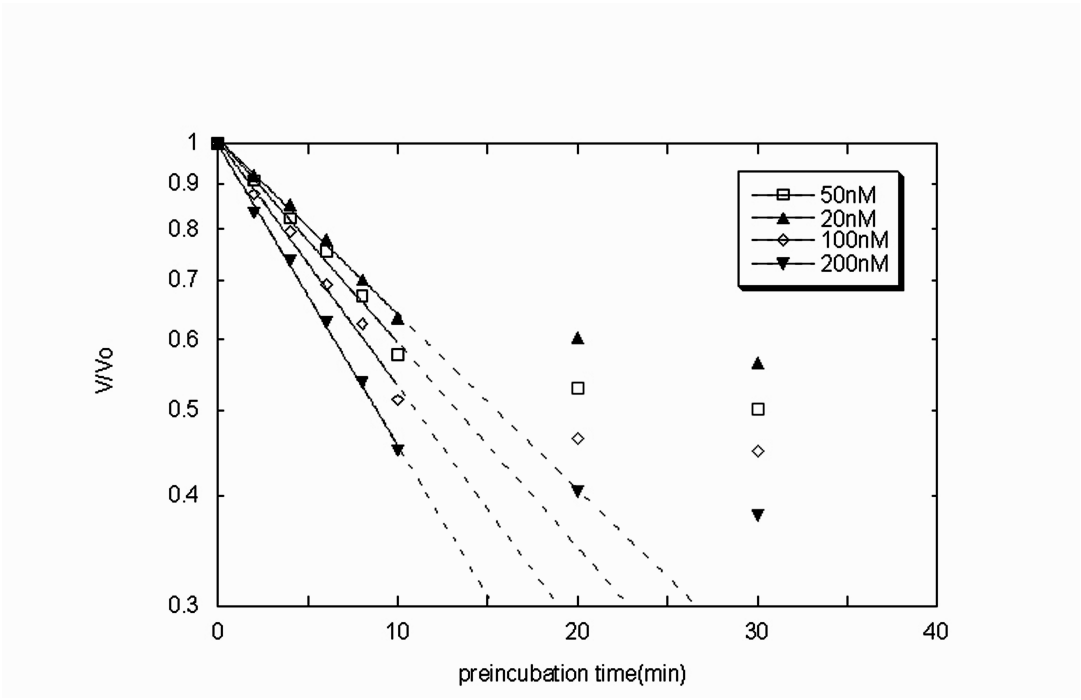

——— y = 1.0107 * e^(-0.045563x) R= 0.99814

– – – y = 1.0135 * e^(-0.053223x) R= 0.99611

— — y = 1.0088 * e^(-0.064032x) R= 0.99607

– – – – – y = 0.99646 * e^(-0.07834x) R= 0.99889

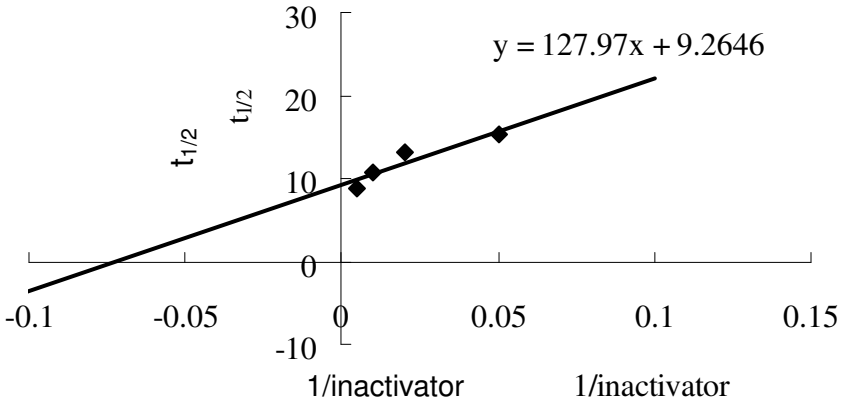

$k_{inact} = 0.0012\ s^{-1}$

$K_i = 13.8$ nM

Figure S8. ESI-MS spectrum of wild type $3CL^{pro}$ m/z values

Different charges got different m/z values (top) and the deconvoluted spectrum, the molecular weight of wild type $3CL^{pro}$ is 33847.35 (bottom).

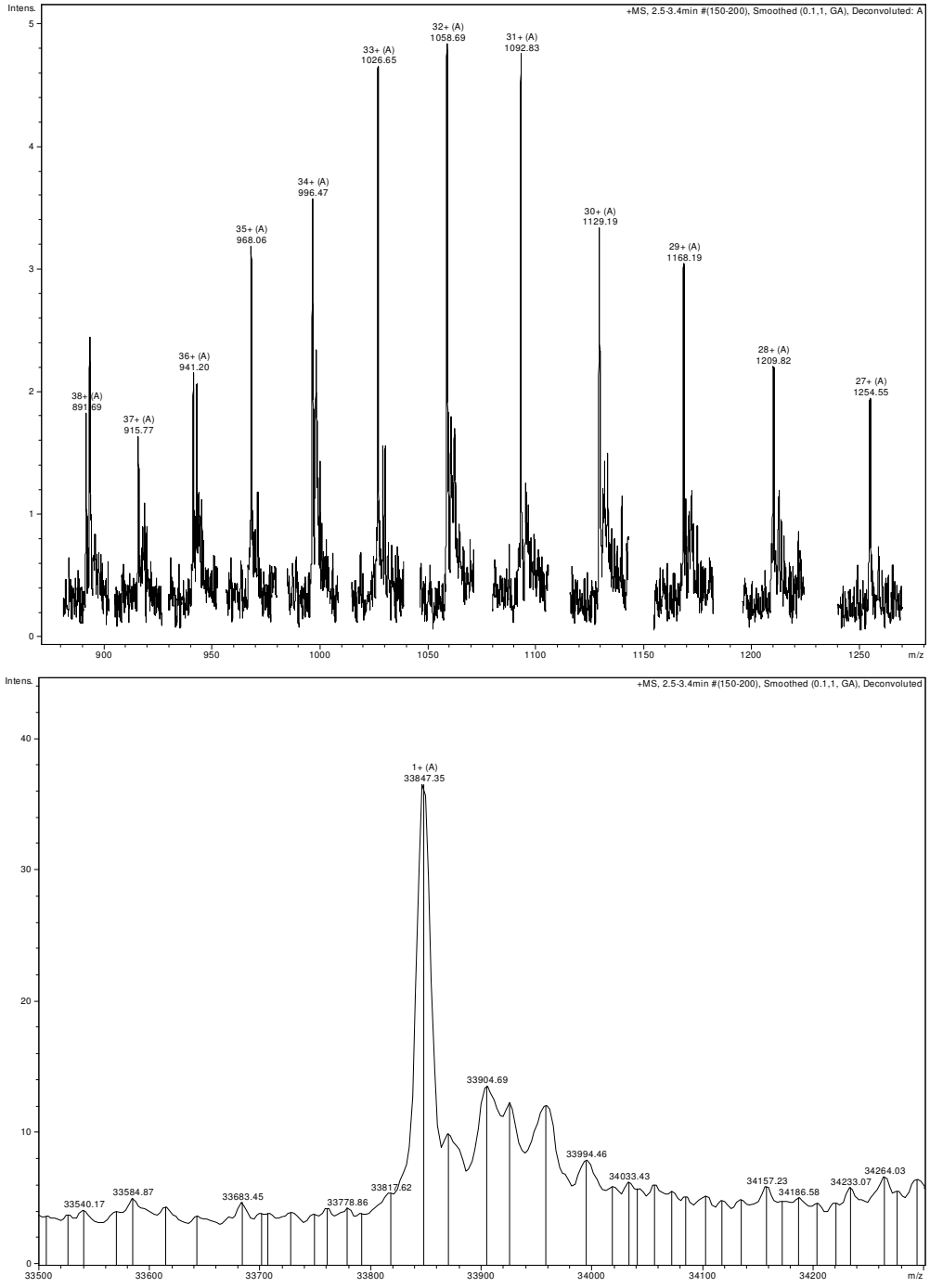

Figure S9. ESI-MS Spectrum of Wild Type 3CL^{pro} Treated with 4-(Dimethylamino)Benzoyl Esters **4** m/z Values

Different charges got different m/z values (top) and the deconvoluted spectrum, the molecular weight of wild type 3CL^{pro} and inhibitor **4** is 33847.35, and the deconvoluted spectrum (bottom).

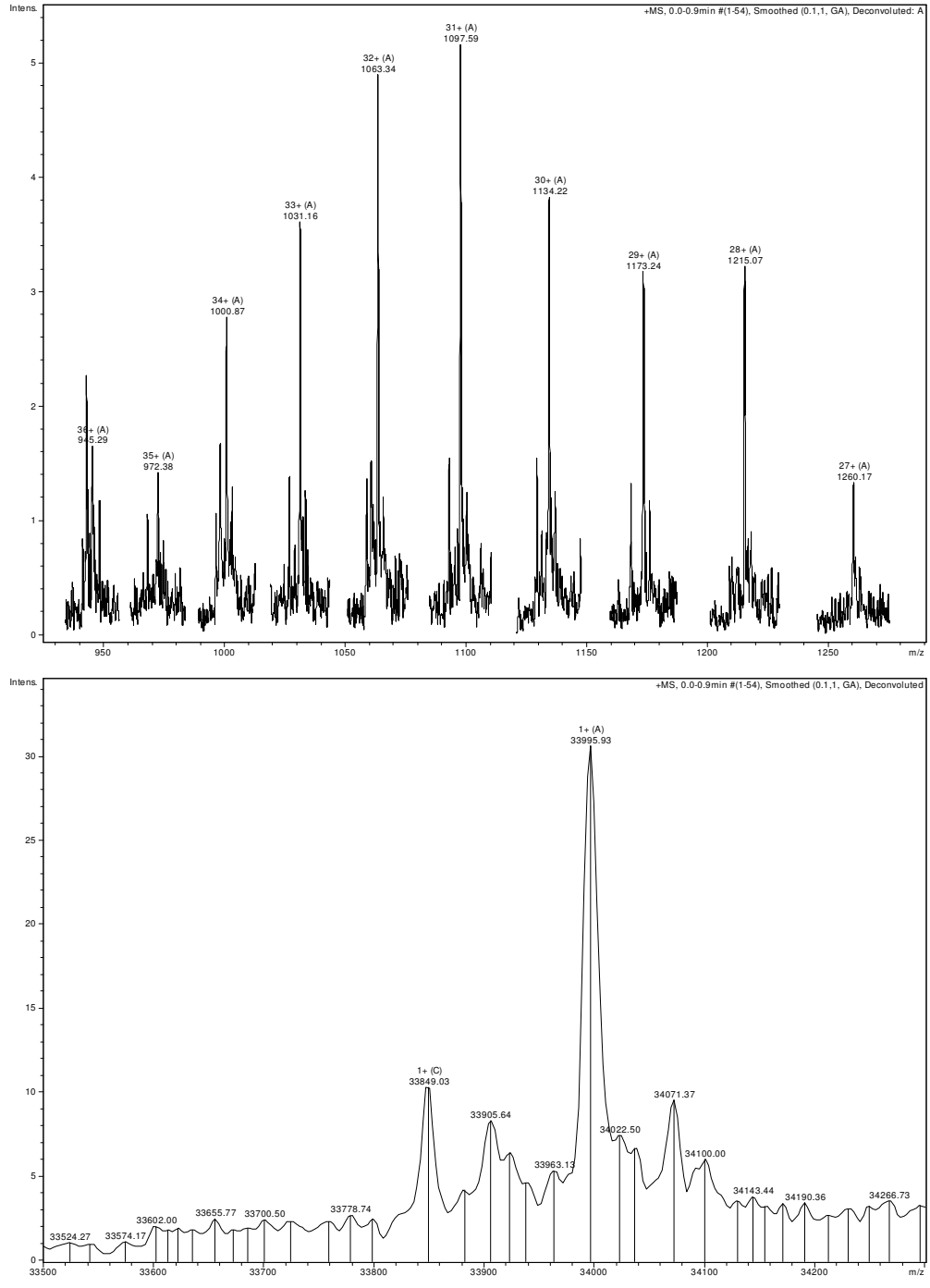

Figure S10. The ORTEP Diagram of Inhibitor **4**

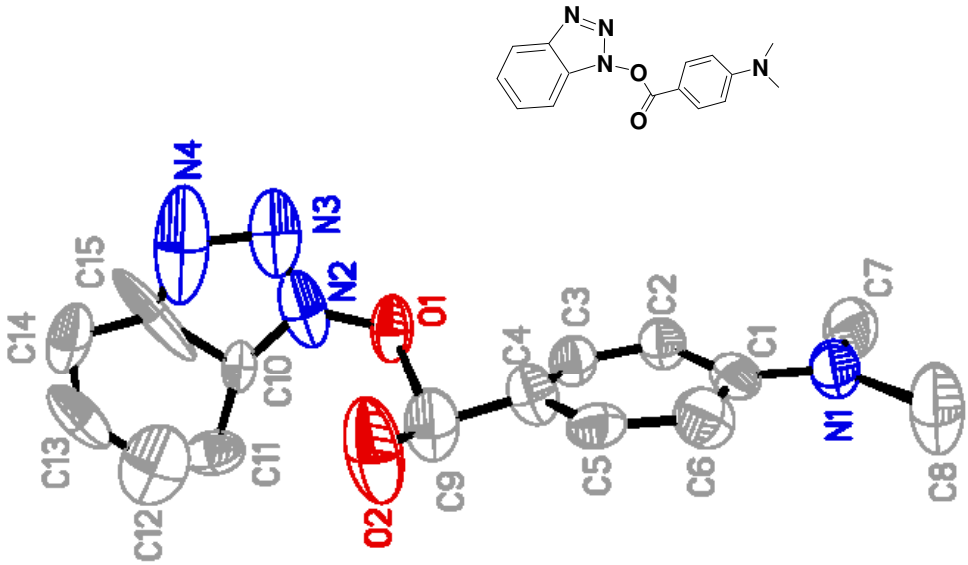

Summary of Crystal Data and Intensity Collection of Inhibitor **4**

Empirical formula	C15 H14 N4 O2	
Diffractometer used	Nonius KappaCCD	
Formula weight	282.30	
Temperature	295(2) K	
Wavelength	0.71073 Å	
Crystal system	Orthorhombic	
Space group	P2(1)2(1)2(1)	
Unit cell dimensions	a = 7.2031(3) Å	□= 90°.
	b = 8.9526(3) Å	□= 90°.
	c = 22.0587(9) Å	□ = 90°.
Volume	1422.49(10) $Å^3$	
Z	4	
Density (calculated)	1.318 Mg/m^3	
Absorption coefficient	0.091 mm^{-1}	
F(000)	592	
Crystal size	0.10 x 0.10 x 0.05 mm^3	
Theta range for data collection	2.97 to 27.49°.	
Index ranges	-9<=h<=9, -11<=k<=11, -26<=l<=28	
Reflections collected	10121	
Independent reflections	3241 [R(int) = 0.1160]	
Completeness to theta = 27.49°	99.3 %	
Absorption correction	Semi-empirical from equivalents	
Max. and min. transmission	0.998 and 0.906	
Refinement method	Full-matrix least-squares on F^2	
Data / restraints / parameters	3241 / 0 / 222	
Goodness-of-fit on F^2	0.995	
Final R indices [I>2sigma(I)]	R1 = 0.1098, wR2 = 0.3096	
R indices (all data)	R1 = 0.2047, wR2 = 0.3897	
Absolute structure parameter	8(8)	
Extinction coefficient	0.07(2)	
Largest diff. peak and hole	0.201 and -0.194 $e.Å^{-3}$	

The crystal has disorder structure and not good data for refinement

Table S1. Bond lengths [Å] and angles [°] for ic11575.

O(2)-C(9)	1.211(5)
N(1)-C(1)	1.357(7)
N(1)-C(8)	1.436(9)
N(1)-C(7)	1.467(9)
C(1)-C(2)	1.406(8)
C(1)-C(6)	1.410(8)
C(2)-C(3)	1.366(8)
C(2)-H(2A)	0.9300
C(3)-C(4)	1.392(8)
C(3)-H(3A)	0.9300
C(4)-C(5)	1.374(8)
C(4)-C(9)	1.484(7)
C(5)-C(6)	1.338(8)
C(5)-H(5A)	0.9300
C(6)-H(6A)	0.9300
C(7)-H(7A)	0.9600
C(7)-H(7B)	0.9600
C(7)-H(7C)	0.9600
C(8)-H(8A)	0.9600
C(8)-H(8B)	0.9600
C(8)-H(8C)	0.9600
C(9)-O(1')	1.3894
C(9)-O(1)	1.7453
O(1)-N(2)	1.3555
N(2)-N(3)	1.2361
N(2)-C(10)	1.3549
N(3)-N(4)	1.3706
N(4)-C(15)	1.1802
C(10)-C(15)	1.4460
C(10)-C(11)	1.6118
C(11)-C(12)	0.9767
C(11)-H(11)	0.9300
C(12)-C(13)	1.3562
C(12)-H(12)	0.9300

C(13)-C(14)	1.3317
C(13)-H(13)	0.9300
C(14)-C(15)	1.3770
C(14)-H(14)	0.9300
O(1')-N(2')	1.4498
N(2')-C(10')	1.2885
N(2')-N(3')	1.3629
N(3')-N(4')	1.1855
N(4')-C(15')	1.5778
N(4')-C(10')	1.9418
C(10')-C(11')	1.5214
C(10')-C(15')	1.7651
C(10')-C(12')	1.8364
C(11')-C(12')	0.9118
C(11')-H(11')	0.9300
C(15')-C(14')	1.3562
C(14')-C(13')	1.3317
C(14')-H(14')	0.9300
C(13')-C(12')	1.3770
C(13')-H(13')	0.9300
C(12')-H(12')	0.9300

C(1)-N(1)-C(8)	120.4(6)
C(1)-N(1)-C(7)	120.7(6)
C(8)-N(1)-C(7)	118.8(6)
N(1)-C(1)-C(2)	121.5(5)
N(1)-C(1)-C(6)	122.1(5)
C(2)-C(1)-C(6)	116.3(5)
C(3)-C(2)-C(1)	120.3(5)
C(3)-C(2)-H(2A)	119.8
C(1)-C(2)-H(2A)	119.8
C(2)-C(3)-C(4)	120.3(5)
C(2)-C(3)-H(3A)	119.9
C(4)-C(3)-H(3A)	119.8
C(5)-C(4)-C(3)	118.5(5)
C(5)-C(4)-C(9)	118.5(5)

C(3)-C(4)-C(9)	121.5(5)
C(6)-C(5)-C(4)	121.4(5)
C(6)-C(5)-H(5A)	119.3
C(4)-C(5)-H(5A)	119.3
C(5)-C(6)-C(1)	121.7(5)
C(5)-C(6)-H(6A)	119.1
C(1)-C(6)-H(6A)	119.1
N(1)-C(7)-H(7A)	109.5
N(1)-C(7)-H(7B)	109.5
H(7A)-C(7)-H(7B)	109.5
N(1)-C(7)-H(7C)	109.5
H(7A)-C(7)-H(7C)	109.5
H(7B)-C(7)-H(7C)	109.5
N(1)-C(8)-H(8A)	109.5
N(1)-C(8)-H(8B)	109.5
H(8A)-C(8)-H(8B)	109.5
N(1)-C(8)-H(8C)	109.4
H(8A)-C(8)-H(8C)	109.5
H(8B)-C(8)-H(8C)	109.5
O(2)-C(9)-O(1')	120.8(3)
O(2)-C(9)-C(4)	124.2(4)
O(1')-C(9)-C(4)	109.1(2)
O(2)-C(9)-O(1)	109.2(4)
O(1')-C(9)-O(1)	33.1
C(4)-C(9)-O(1)	98.7(3)
N(2)-O(1)-C(9)	119.2
N(3)-N(2)-C(10)	115.8
N(3)-N(2)-O(1)	116.9
C(10)-N(2)-O(1)	125.3
N(2)-N(3)-N(4)	96.5
C(15)-N(4)-N(3)	123.9
N(2)-C(10)-C(15)	103.0
N(2)-C(10)-C(11)	150.3
C(15)-C(10)-C(11)	105.7
C(12)-C(11)-C(10)	120.5
C(12)-C(11)-H(11)	119.7

C(10)-C(11)-H(11)	119.7
C(11)-C(12)-C(13)	131.2
C(11)-C(12)-H(12)	114.4
C(13)-C(12)-H(12)	114.4
C(14)-C(13)-C(12)	124.0
C(14)-C(13)-H(13)	118.0
C(12)-C(13)-H(13)	118.0
C(13)-C(14)-C(15)	109.6
C(13)-C(14)-H(14)	125.2
C(15)-C(14)-H(14)	125.2
N(4)-C(15)-C(14)	132.5
N(4)-C(15)-C(10)	99.2
C(14)-C(15)-C(10)	128.3
C(9)-O(1')-N(2')	106.2
C(10')-N(2')-N(3')	98.2
C(10')-N(2')-O(1')	137.2
N(3')-N(2')-O(1')	123.6
N(4')-N(3')-N(2')	108.6
N(3')-N(4')-C(15')	134.5
N(3')-N(4')-C(10')	75.4
C(15')-N(4')-C(10')	59.1
N(2')-C(10')-C(11')	112.8
N(2')-C(10')-C(15')	126.8
C(11')-C(10')-C(15')	120.1
N(2')-C(10')-C(12')	142.5
C(11')-C(10')-C(12')	29.7
C(15')-C(10')-C(12')	90.6
N(2')-C(10')-N(4')	76.9
C(11')-C(10')-N(4')	170.1
C(15')-C(10')-N(4')	50.1
C(12')-C(10')-N(4')	140.6
C(12')-C(11')-C(10')	94.7
C(12')-C(11')-H(11')	132.7
C(10')-C(11')-H(11')	132.7
C(14')-C(15')-N(4')	173.4
C(14')-C(15')-C(10')	105.5

N(4')-C(15')-C(10')	70.8
C(13')-C(14')-C(15')	124.0
C(13')-C(14')-H(14')	118.0
C(15')-C(14')-H(14')	118.0
C(14')-C(13')-C(12')	109.6
C(14')-C(13')-H(13')	125.2
C(12')-C(13')-H(13')	125.2
C(11')-C(12')-C(13')	165.3
C(11')-C(12')-C(10')	55.7
C(13')-C(12')-C(10')	110.0
C(11')-C(12')-H(12')	97.3
C(13')-C(12')-H(12')	97.3
C(10')-C(12')-H(12')	150.3

Symmetry transformations used to generate equivalent atoms:

Computer Modeling of SARS-CoV 3CL Protease Inhibition.

Docking was performed by using Autodock version 3.05 [S6]. The crystal structure of SARS-CoV 3CL protease in complex with a substrate-analogue inhibitor (coded 1uk4) was obtained from The Protein Databank (PDB; http://www.rcsb.org/pdb/). The bound CMK peptide, water molecules (except HOH_16), and chain B were removed from the original PDB file. Compound structures were drawn in CAChe (Fujitsu, Japan) and refined by performing an optimized geometry calculation in mechanics using augmented MM2 parameters. The target structure (1uk4 chain A) was first added essential hydrogen atoms, assigned Kollman united atom charges [S7], and given solvation parameters before docking study. Compound molecules were added all polar hydrogen atoms, assigned Gasteiger-Marsili charges [S8] and defined torsions. Pre-computed energy grid maps with grid point spacing of 0.375A and 50X50X50 grid points centered at the active site were used (autogrid tool in Autodock3.05). During a docking experiment, each compound was kept flexible (except their rings and amide bonds) and the built-in Lamarckian genetic algorithm (LGA) and Solis & Wets local search method was adopted. The local search used 0.5-Å quaternion and 5^{o} torsion steps. In each compound structure, 1.5×10^{6} energy were evaluated and 50 poses were selected from 2.7×10^{5} generations per run. MGLTOOLS (MGL, Scripps Institute) was used for model visualization, docking parameters preparation, and results presentation. A python script was programmed to assist to collecting binding energies, selecting minima, and clustering structures within 2 Å root mean square deviation (RMSD) from the results of all job runs.

Experimental and estimated binding free energy were derived from the docking simulation.

Inhibitor	Molecular weight	K_i (nM)	-ΔG (kcal/mol)	-ΔG*[a] (kcal/mol)	DM (debye)	IP[b] (eV)	EA[b] (eV)	GAP[b] (eV)
3	254.248	19.5	9.611	8.13	4.400	8.538	2.815	5.724
4	282.301	17.4	9.851	8.16	6.066	8.309	2.372	5.937
5	268.274	12.1	9.030	8.02	5.959	8.381	2.409	5.972
6	310.355	11.1	9.006	8.48	6.388	8.318	2.344	5.974
7	279.257	22.9	8.841	8.15	6.848	8.963	2.684	6.279
8	278.270	7.5	8.758	8.17	5.517	8.682	2.587	6.095
9	278.270	12.3	8.234	8.06	3.347	8.673	2.009	6.664
10	296.260	13.8	7.823	8.23	3.347	8.878	2.154	6.724
14	308.382	1000		7.94	6.152	8.215	0.878	7.337
17	266.302	4500		7.83	6.129	8.282	0.913	7.369
18	280.329	6700		7.20	6.121	8.206	0.891	7.315

(a) ΔG^* is computed by AUTODOCK3.0.5 (b) IP, the ionization potential of the molecular geometry, is approximated by the energy of the highest occupied molecular orbital (HOMO); EA, the electron affinity, is approximated by the energy of the lowest unoccupied molecular orbital (LUMO); GAP = IP-EA. All values are obtained after optimizing the molecular geometry using Augmented MM2 followed by MOPAC with PM3 parameters [S9].

DM, the dipole moment, is calculated by MOPAC using PM3 parameters at a molecular mechanics minimum energy geometry determined by optimization using Augmented MM2 [S9].

Supplemental References

S1. Copeland, R. A. Copeland, (2000). Enzymes, WILEY-VCH, Inc, USA, pp. 318-349.

S2. Kuo, C.-J., Chi, Y.-H., Hsu, T.-A., and Liang, P.-H. (2004). Characterization of SARS main protease and inhibitor assay using a fluorogenic substrate. Biochem. Biophys. Res. Commun. *318*, 862-867.

S3. Wu, C.-Y., Jan, J.-T., Ma, H.-H., Kuo, C.-J., Juan, H.-F., Cheng, Y.-S.E., Hsu, H.-H., Huang, H.-C., Wu, D., Brik, A. et al. (2004). Small molecules targeting severe acute respiratory syndrome human coronavirus. Proc. Natl. Acad. Sci. U. S. A. *101*, 10012-10017.

S4. Hsu, J.T.-A., Kuo, C.-J., Hsieh, H.-P., Wang, Y.-C., Huang, K.-K., Lina, C.P.-C., Huang, P.-F., Chen, X., and Liang, P.-H. (2004) Evaluation of metal-conjugated compounds as inhibitors of 3CL protease of SARS-CoV. FEBS Lett. *574*, 116-120.

S5. Kitz, R., and Wilson, I.B. (1962). Esters of methanesulfonic acid as irreversible inhibitors of acetylcholinesterase. J. Biol. Chem. **1962**, *237*, 3245–3249.

S6. Morris, G.M., Goodsell, D.S., Halliday, R.S., Huey, R., Hart, W.E., Belew, R.K., and Olsen, A.J. (1998) Automated docking using a Lamarckian genetic algorithm and an empirical binding free energy function. J. Comput. Chem. *19*, 1639-1662.

S7. Weiner, S.J., Kollman, P.A., Case, D.A., Singh, U.C., Ghio, C., Alagona, G., Profeta, S., and Weiner, P. (1984). A new force field for molecular mechanical simulation of nucleic acids and proteins. J. Am. Chem. Soc. *106*, 765–784.

S8. Gsateiger, J., and Marsili, M. (1980). Iterative partial equalization of orbital electronegativity-a rapid access to atomic charges. Tetrahedron *36*, 3219–3288.

S9. Stewart, J. J. P. (1989) Optimization of parameters for semiempirical methods. II. applications. J. Comput. Chem. *1*